A Strain-Driven Moment-Curvature Analysis of Composite Cross-Sections Exposed to Fire

C. G. Chiorean[1], L. Imre[1] and R. A. M. Silveira[2]

[1]Department of Structural Mechanics, Technical University of Cluj-Napoca, Cluj-Napoca, Romania
[2]Dept. of Civil Engineering School of Mines, Federal University of Ouro Preto, Ouro Preto, MG, Brazil

Abstract

This paper presents a novel strain-driven incremental-iterative procedure for moment-curvature analysis of composite steel concrete cross-sections of arbitrary shape exposed to fire. The equilibrium equations are expressed in terms of prescribed axial force and bending moment ratio, while the inelastic behaviour and the solution are controlled at the fibre level, enhancing the global convergence properties of the entire process. The distinctive features of the strain-driven approach outlined here include its ability to accurately capture all critical points on the complete moment-curvature diagrams and eliminate the need for specialized load-path numerical strategies to address singular points associated with ultimate strength capacity. The validation process involves comparisons with other numerical results and experimental data from international literature, extending also the benchmark results used for strength capacity assessment and moment-curvature diagrams of composite cross-sections exposed to high temperatures.

Keywords: fire analysis, moment-curvature analysis, composite-cross-section, biaxial bending, strain-softening, nonlinear analysis.

1   Introduction

The combined effect of bi-axial bending and axial force is one of the main critical solicitations for vertical structural elements, particularly during fires, as they significantly impact strength and stability. Elevated temperatures during fires alter the mechanical properties of structural elements, leading also to additional thermal

strains due to thermal expansion. These thermal effects, combined with bi-axial bending and axial forces, can worsen the effects of fire, increasing the risk of failure. Accurate evaluations of cross-sectional strength are essential during both design phases and advanced nonlinear analyses to ensure fire-resistant structures capable of withstanding thermal-induced loads and stresses. However, assessing the strength capacity of composite cross-sections exposed to fire poses computational challenges due to their complex and nonlinear behaviour. Computational efficiency is crucial for conducting these evaluations within reasonable timeframes, requiring the use of efficient numerical methods and algorithms. Current standards [1-3] provide simplistic calculation methods for assessing reinforced concrete sections in fire, lacking provisions for bi-axially loaded composite cross-sections. This necessitates the development of efficient computational models to evaluate the biaxial bending failure of composite cross-sections in fire, driving on-going research efforts to create advanced and practical models considering the effect of elevated temperatures on the inelastic behaviour of various structural elements [4, 5]. A comprehensive understanding of the inelastic behaviour of cross-sections under bi-axial bending and axial force can be achieved through moment-curvature analysis, typically denoted as *M-N-ϕ*. There are two fundamental approaches to perform such analysis. The first approach, a deformation-driven algorithm$(M_\theta - N - \phi)$, aims to evaluate bending moments corresponding to a given total curvature while maintaining a constant inclination of the neutral axis ($\tan\theta = \frac{\phi_y}{\phi_z}$) (e.g. [4, 6]). Although, such approaches exhibits relatively well numerical stability, may introduce spurious bending moments for arbitrary cross-section shapes, resulting in inaccuracies in representing in the same plane moment-curvature diagram of the cross-sections with arbitrary shape. The second approach, denoted as $(M_\alpha - N - \phi)$, involves solving nonlinear equilibrium equations for axial force and prescribed bending moment ratio ($\tan\alpha = \frac{M_y}{M_z}$) according to the classical Newton's scheme (e.g. [7, 8]). Although this approach can provide informative diagrams regarding yielding, load-carrying capacity, and failure mode, it is time-consuming, prone to convergence issues, and sensitive to initial approximations (i.e. starting point dependent), particularly for non-symmetric cross-sections or those subjected to high axial forces. Recent enhancements, to improve convergence and accuracy, include the adoption of Newton-Raphson iterative procedures in conjunction with advanced path-following strategies [8] controlling in this way the nonlinear solution in both forces and deformations and solving the three coupled nonlinear equilibrium equations even in post-critical domain. Nonetheless, satisfying the basic equilibrium equations can still be challenging, especially for complex cross-sections with non-symmetric shapes or when axial force falls outside the iso-load contour [7].

This study introduces a novel strain-driven incremental-iterative method for determining the complete moment-curvature response of composite steel-concrete cross-sections with arbitrary shapes exposed to elevated temperatures. The diagrams are determined such that axial force and bending moment ratio are kept constant$(M_\alpha - N - \phi)$, for a continuously increasing the prescribed value of the strain in cross-section's most compressed/tensioned point. By manipulating the three

coupled nonlinear equilibrium equations, one equation can be uncoupled, reducing the iterative numerical process to just two coupled nonlinear equations. This approach, utilizing a damped Newton iterative strategy with a non-singular Jacobian, offers several advantages: (*i*) controlling the solution at the fiber level ensures numerical stability and prevents divergence, ensuring global convergence; (*ii*) critical points on the moment-curvature diagrams can be accurately captured; (*iii*) no special load-path numerical strategies are required to handle singular points associated with ultimate strength capacity. Numerical studies demonstrate the effectiveness of the proposed methodology in determining complete moment-curvature relationships, including strength reduction beyond multiple peak points and degradation of cross-section rigidity at different loading stages.

2   Mathematical formulation

A strain-driven incremental-iterative method is proposed herein in order to determine the complete moment-curvature response of composite steel-concrete cross-sections with arbitrary shapes exposed to elevated temperatures.

2.1   Basic assumptions

Consider the composite cross-section subjected to the action of the external bending moment $\vec{\mathbf{M}}_O = M_z\vec{\mathbf{i}} + M_y\vec{\mathbf{j}}$ with scalar components (M_z, M_y) applied about global axes Oz (with unit vector $\vec{\mathbf{i}}$) and Oy (with unit vector $\vec{\mathbf{j}}$) respectively, and axial force $\vec{\mathbf{N}} = N\vec{\mathbf{k}}$ with scalar component (N) applied along the Ox axis (with unit vector $\vec{\mathbf{k}}$) as shown in Fig. 1a, where the origin O of the Cartesian reference axes could be arbitrarily selected. Usually, the origin O is selected as either geometrical or plastic centroid of the cross-section. The cross-section may assume any shape with multiple polygonal or circular openings. However, the approach described in this paper is limited to composite steel-concrete sections in which the structural steel is partly or fully enclosed within concrete. It is assumed that plane section remains plane after deformation. Thus, at the ambient temperatures, the resultant strains distribution corresponding to the curvatures about each global axes collected in resultant curvature vector $\vec{\mathbf{\Phi}} = \begin{bmatrix} \phi_z & \phi_y \end{bmatrix}^T = \phi_z\vec{\mathbf{i}} + \phi_y\vec{\mathbf{j}}$ and the axial strain u can be expressed in a linear form at a generic point of coordinates (z, y) defined by the vector $\vec{\mathbf{r}} = \begin{bmatrix} z & y \end{bmatrix}^T = z\vec{\mathbf{i}} + y\vec{\mathbf{j}}$, in any fiber of concrete matrix, structural steel or ordinary reinforced bars. In fire conditions, the implicit nonlinear constitutive models both for steel and concrete are considered, and thermal transient and creep strains are implicitly included in nonlinear constitutive models adopted for steel and concrete [1-5]. As a consequence, the total strain comprises only mechanical and thermal strain. Although an approximation, it is assumed that the *total strain field* varies linearly throughout the cross-section and with the above notations may be expressed in vectorial form as (Fig. 1b):

$$\vec{\mathbf{\varepsilon}}_{tot}(\vec{\mathbf{r}}) = u\vec{\mathbf{k}} + \vec{\mathbf{\Phi}} \times \vec{\mathbf{r}} = \varepsilon_{tot}\vec{\mathbf{k}} \tag{1}$$

where $\times$ denotes the vector product. Such an assumption is in line with Bernoulli plane section hypothesis, an assumption acceptable even at elevated temperatures, and has been employed successfully in other advanced numerical formulations [4, 5,

3

9]. As a result of the aforementioned assumption, for a given fiber (steel or concrete), the total strain is assumed to follow an additive decomposition of mechanical and thermal strain as:

$$\varepsilon_{tot}\left(u, \phi_z, \phi_y; T\right) = u + \phi_z y - \phi_y z = \varepsilon_{mech} + \varepsilon_{th}(T) \tag{2}$$

where ε_{mech} represents the mechanical strain and ε_{th} represents the thermal strain which depends on temperature the T at the specified fiber. The thermal strains for concrete may be determined distinctively in function of the aggregate types and in this paper the values for concrete and steel are assumed according with the values given in Eurocode 2 [1]. From Eq. (2) the mechanical strain can be expressed as:

$$\varepsilon_{mech}\left(u, \phi_z, \phi_y; T\right) = \varepsilon_{tot} - \varepsilon_{th} \tag{3}$$

and the implicit nonlinear constitutive material model for concrete and steel at high temperatures can be defined in the following way:

$$\vec{\boldsymbol{\sigma}}(\vec{\mathbf{r}}) = \sigma \vec{\mathbf{k}}$$
$$\sigma = \sigma(\varepsilon_{mech}; T) \tag{4}$$
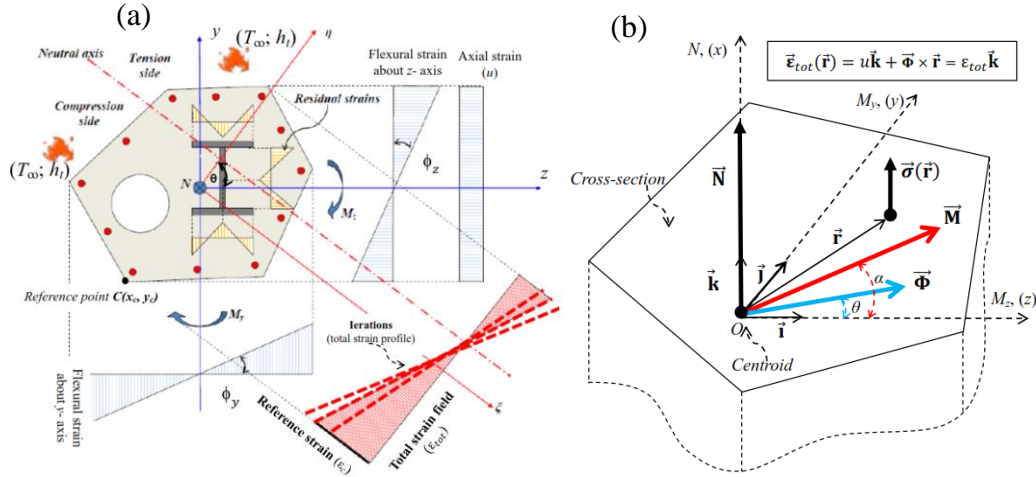
Figure 1: (a) Model of composite cross-section; (b) Positive sign convention and total strain field definition.

In this paper, moisture effects and all the material properties, both thermal and mechanical, are assumed according to European Standards [1-3] but other nonlinear constitutive relationships may be easily accommodated in the present formulation. It is important to highlight that the important effect of the spalling of concrete at elevated temperatures is not considered in the present formulation. However, since the proposed approach involves a *sequentially coupled thermal-stress analysis*, hence the mechanical problem is solved after the thermal analysis has been performed; the effects of spalling may be implicitly added to the mechanical analysis by means of performing explicit pore-pressure analyses and coupled with the thermal analysis to determine the temperature field throughout the cross-section and hence the proposed mechanical analysis basically applies in the same way, and the computational efficiency of the proposed method, that it is the main goal of the proposed study, will not be affected. In the thermal analysis reinforcement bars are neglected, with the temperatures of the bars considered equal with the surrounding

concrete temperature and also it is assumed continuity in terms of temperature at the interface between structural steel and concrete matrix, although more elaborative models may be considered to treat the air gap effect between the steel and concrete [10].

2.2 Proposed numerical formulation

The analysis method is carried out in two main steps: (*i*) thermal analysis, used to evaluate the temperature distribution field throughout the cross-section at a specific time, as will be briefly described below and (*ii*) mechanical analysis, in which the moment-curvature diagrams are determined.

2.2.1 Thermal analysis

For a given cross-section, the thermal analysis is performed by solving the 2-D heat conduction equation:

$$k\nabla^2 T = \rho c \frac{\partial T}{\partial t} \tag{5}$$

where k is the thermal conductivity, c is the specific heat and ρ is the mass density of material, t represents time, and T represents temperature. At the surface of the cross-section, heat exchange between surface and ambient air occurs through heat convection and radiation, the effect of convective and radiative boundary conditions is considered as:

$$k\nabla T \mathbf{n} = h_c(T - T_\infty) + \varepsilon_r \sigma(T^4 - T_\infty{}^4) \tag{6}$$

where T_∞ is the ambient (gas) temperature, h_c is the convective heat transfer coefficient, n is the vector normal to the boundary; ε_r is resultant emissivity and $\sigma=5.67\times10\text{-}8\text{W/m2K4}$ is the Stephan Boltzmann constant. Introducing the radiative heat transfer coefficient as:

$$h_r = \varepsilon_r \sigma(T^2 - T_\infty{}^2) \cdot (T - T_\infty) \tag{7}$$

the above relationship (6) may be also expressed as:

$$k\nabla T \mathbf{n} = h_c(T - T_\infty) + h_r(T - T_\infty) = h_t(T - T_\infty) \ ; h_t = h_c + h_r \tag{8}$$

where h_t represents a total heat transfer coefficient through convection and radiation. It should be noted that this coefficient is not constant during the thermal action of the fire because the radiative heat transfer coefficient h_r is defined based on the surface temperature of the body surface at a certain moment of exposure, so it is a function of temperature. The initial conditions consist of the temperature of every point throughout the cross-section at the beginning of the analysis $T(y, z, t_0) = T_0$ (*y, z*) where the temperature T_0 is specified. In the FEM context in which the above mentioned transient heat transfer problem is solved, the equilibrium equation is described as:

$$\mathbf{C}\{\partial \mathbf{T}/\partial t\} + \mathbf{K}\{\mathbf{T}\} = \mathbf{R} \tag{9}$$

where **C**, **K** and **R** are the capacitance matrix (thermal capacity), the thermal conductivity matrix and the nodal heat flux vector, defined according to:

$$\mathbf{C} = \int_\Omega \rho c \mathbf{N}^T \mathbf{N} d\Omega; \ \mathbf{K} = \int_\Omega \mathbf{B}^T \mathbf{D} \mathbf{B} d\Omega + h_t \int_\Gamma \mathbf{N}^T \mathbf{N} d\Gamma \ ; \mathbf{R} = h_t T_\infty \int_\Gamma \mathbf{N}^T \, d\Gamma \tag{10}$$

with **B** being the matrix containing the derivatives of the interpolation functions, **N** is the matrix containing the interpolation shape functions, and **D** is the thermal

conductivity matrix. The standard ISO 8364 fire curve is used in this paper to obtain the gases temperature:

$$T_\infty = 20 + 345 log_{10}(8t + 1)$$

(11)

where T_∞ is the gas temperature (^{0}C) and t is the time of exposure to fire in minutes. To solve the Eq. (9) an explicit numerical time integration strategy based on the finite difference Crank-Nicolson method is adopted. To address the heat transfer of composite steel-concrete cross-sections, the computer program incorporated two types of triangular finite elements, one with 3 nodes and one with 6 nodes, and different numbers of integration points. In the mechanical analysis, the surface integrals will be assessed using the identical mesh. Since the Eq. (9) is strongly nonlinear due to the dependence on temperature of both the thermal properties and the radiative component h_r, an incremental-iterative procedure has been implemented in the developed computer program.

2.2.2 Moment curvature analysis: general procedure

In order to determine the moment curvature diagrams of composite steel concrete cross-sections subjected to axial force and given bending moment ratio ($\tan(\alpha) = M_y/M_z$), a strain-driven algorithm is developed and the full moment-curvature diagram is computed by continuously monitoring the strain in the referenced concrete fibre of cross-section. In this respect, the incremental-iterative procedure previously developed in [7] for ambient temperature is extended here for elevated temperatures. Consider a composite cross-section with arbitrary shape as shown in Fig. 1a subjected to biaxial bending moments (λM_{z0}, λM_{y0}) and axial force (N_0), where λ represents the load factor multiplying the reference bending moments M_{z0} and M_{y0}. The global z, y -axes of the cross section can have arbitrary origin, but usually is selected as the plastic centroid computed at ambient temperature. The equilibrium is achieved when the external forces (N_0, λM_{z0}, and λM_{y0}) are equal to the internal ones. These conditions can be represented mathematically in terms of the following nonlinear system of equations as:

$$\begin{cases} \int_\Omega \sigma\left(\varepsilon_{mech}\left(u, \phi_z, \phi_y\right)\right) d\Omega + \sum_{b=1}^{N_b} \sigma\left(\varepsilon_{mech,b}\left(u, \phi_z, \phi_y\right)\right) A_{r,b} - N_0 = 0 \\ \int_\Omega \sigma\left(\varepsilon_{mech}\left(u, \phi_z, \phi_y\right)\right) y d\Omega + \sum_{b=1}^{N_b} \sigma\left(\varepsilon_{mech,b}\left(u, \phi_z, \phi_y\right)\right) y_b A_{r,b} - \lambda M_{z0} = 0 \quad (12) \\ -\int_\Omega \sigma\left(\varepsilon_{mech}\left(u, \phi_z, \phi_y\right)\right) z d\Omega - \sum_{b=1}^{N_b} \sigma\left(\varepsilon_{mech,b}\left(u, \phi_z, \phi_y\right)\right) z_b A_{r,b} - \lambda M_{y0} = 0 \end{cases}$$

where A_{rb} ($b=1,N_b$) denotes the resisting cross-section area of the i-th bar located at (z_b, y_b) coordinates about the reference system (zOy), N_b denotes the total number of conventional steel reinforcements, with the surface integral extended over steel and concrete areas, and u, ϕ_z, ϕ_y represent the main unknowns. Although such a system may be solved using different load control approaches (i.e. varying the load factor λ) combined with Newton iterative method (e.g. arc-length family methods), a strain driven approach, as detailed herein, can be more effective from the following reasons: (*i*) the numerical stability and divergence situations may be efficiently controlled enhancing the global convergence properties of the entire process, since the solution is controlled at the fibre level; (*ii*) different critical points on the

6

moment curvature diagrams (i.e. maximum bending moment or bending moment associated to a prescribed value of ultimate strain) may be efficiently captured with a great accuracy; (*iii*) no special load-path numerical strategies are needed to treat the singular points associated to ultimate strength capacity (i.e. maximum bending moment). One point on the moment curvature diagram correspond to a prescribed value of the reference strain, usually defined at the most compressed/tensioned point of the concrete section (i.e. $\varepsilon_{c,max}$ equal to the prescribed value of compressive strain ε_c). Considering the irregular composite section as shown in Fig. 1a, the orientation of the neutral axis may be defined by the curvatures ϕ_z and ϕ_y. For each orientation of the neutral axis, $tan\theta = \dfrac{\phi_y}{\phi_z}$, the rate of change of the total strain field $\vec{\varepsilon}_{tot}$ in the direction of the resultant curvature vector $\overrightarrow{\Phi}_{rez}$ may be computed as directional derivative of the total strain field along the unit vector of $\overrightarrow{\Phi}_{rez}$ for each concrete vertex (i.e. the original corner points of the initial polygon, before the mesh is applied, that defines the cross-section) of coordinates (z, y) as:

$$\mathbf{n}_{\Phi_{rez}} \nabla \vec{\varepsilon}_{tot} = \frac{\partial \varepsilon_{tot}}{\partial \phi_z} cos\bar{\theta} + \frac{\partial \varepsilon_{tot}}{\partial \phi_y} sin\bar{\theta} = ycos\bar{\theta} - zsin\bar{\theta} \tag{13}$$

where $\vec{\mathbf{n}}_{\Phi_{rez}} = cos\bar{\theta}\mathbf{i} + sin\bar{\theta}\mathbf{j}$ is the unit vector of the resultant vector $\overrightarrow{\Phi}_{rez} = \overrightarrow{\Phi} + \overrightarrow{\Phi}_0 = \left(\phi_z + \phi_{z0}\right)\mathbf{i} + \left(\phi_y + \phi_{y0}\right)\mathbf{j}$, in which ϕ_{z0}, ϕ_{y0} represents the components of the initial curvature vector $\overrightarrow{\Phi}_0$ associated to a total bending moment equal to zero, $\nabla\vec{\varepsilon}_{tot}$ represents the gradient of the total strain field as defined in Eqs. (1), (2). In this way the concrete vertex with the lowest rate of change may be identified and considered further as a reference point with coordinates (z_c, y_c), as illustrated in Fig. 1a. It is worth noting that the curvature components ϕ_{z0}, ϕ_{y0} are zero for symmetrical cross-sections or when the cross-section is referenced about a true plastic centroid as will be detailed in the next section of the paper. Assuming the prescribed value ε_c^p for the strain at this point, the axial strain *u* can be expressed as:

$$u + \phi_z y_c - \phi_y z_c = \varepsilon_c^p \tag{14}$$

$$u = \varepsilon_c^p - \left(\phi_z y_c - \phi_y z_c\right) \tag{15}$$

and then by combining the Eq.(15) and (2), the resulting total strain distribution corresponding to the curvatures ϕ_z and ϕ_y can be expressed in linear form as:

$$\tilde{\varepsilon}_{tot}\left(\phi_z, \phi_y\right) = \varepsilon_c^p + \phi_z(y - y_c) - \phi_y(z - z_c) \tag{16}$$

and the mechanical strain field may be also rewritten as:

$$\tilde{\varepsilon}_{mech}\left(\phi_z, \phi_y\right) = \tilde{\varepsilon}_{tot}\left(\phi_z, \phi_y\right) - \varepsilon_{th}(T) \tag{17}$$

Therefore, considering a given bending moment ratio (tan(α)= M_y/M_z) the basic equations of equilibrium (12) can be decoupled and written in the following form:

$$\begin{cases} f_1\left(\phi_z, \phi_y; \varepsilon_c^p\right) = \int_\Omega \sigma\left(\tilde{\varepsilon}_{mech}\left(\phi_z, \phi_y\right)\right) d\Omega + \sum_{b=1}^{N_b} \sigma\left(\tilde{\varepsilon}_{mech,b}\left(\phi_z, \phi_y\right)\right) A_{r,b} - N_0 = 0 \\ f_2\left(\phi_z, \phi_y; \varepsilon_c^p\right) = \int_\Omega \sigma\left(\tilde{\varepsilon}_{mech}\left(\phi_z, \phi_y\right)\right) z d\Omega + \sum_{b=1}^{N_b} \sigma\left(\tilde{\varepsilon}_{mech,b}\left(\phi_z, \phi_y\right)\right) z_b A_{r,b} + \\ \quad +\tan(\alpha)\left(\int_\Omega \sigma\left(\tilde{\varepsilon}_{mech}\left(\phi_z, \phi_y\right)\right) y d\Omega + \sum_{b=1}^{N_b} \sigma\left(\tilde{\varepsilon}_{mech,b}\left(\phi_z, \phi_y\right)\right) y_b A_{r,b}\right) = 0 \end{cases} \tag{18}$$

in which the curvatures ϕ_z, ϕ_y becomes the main unknowns and then the bending moment about z-axis may be simply evaluated as:

$$M_z = \int_\Omega \sigma\left(\tilde{\varepsilon}_{mech}\left(\phi_z, \phi_y\right)\right) y d\Omega + \Sigma_{b=1}^{N_b} \sigma\left(\tilde{\varepsilon}_{mech,b}\left(\phi_z, \phi_y\right)\right) y_b A_{r,b} \qquad (19)$$

The two coupled nonlinear equations (18) may be expressed analytically in matrix form as:

$$\mathbf{F}\left(\mathbf{\Phi}; \varepsilon_c^p\right) = \mathbf{0}; \qquad (20a)$$

$$\mathbf{F} = \left[f_1\left(\phi_z, \phi_y; \varepsilon_c^p\right), f_2\left(\phi_z, \phi_y; \varepsilon_c^p\right)\right]^T ; \mathbf{\Phi} = \left[\phi_z, \phi_y\right]^T \quad (20b)$$

which may be solved by means of applying a damped-Newton method [11]:

$$\mathbf{\Phi}^{k+1} = \mathbf{\Phi}^k + \lambda^k \boldsymbol{\delta}^k \qquad (21a)$$

$$\boldsymbol{\delta}^k = -\mathbf{J}\left(\mathbf{\Phi}^k; \varepsilon_c^p\right)^{-1} \cdot \mathbf{F}\left(\mathbf{\Phi}^k; \varepsilon_c^p\right) \qquad (21b)$$

$$\nabla F^k = \mathbf{F}\left(\mathbf{\Phi}^k; \varepsilon_c^p\right) \mathbf{J}\left(\mathbf{\Phi}^k; \varepsilon_c^p\right) \qquad (21c)$$

where $\mathbf{J} = \frac{\partial \mathbf{F}}{\partial \mathbf{\Phi}}$ represents the Jacobian of the coupled equations of the system (18) and $\lambda^k \in (0,1]$ is the backtracking line search parameter used to compute the step length [11]. The Jacobian of the above nonlinear equation system is always non-singular since relates the changes of the prescribed axial force, always kept lower than its maximum value (the peak value in the N-M space), with the strain field that defines a bending moment ratio [11]. Hence, for a given value of axial force N_0, a prescribed strain ε_c^p for the reference strain, and a given bending moment ratio, $\tan(\alpha)$, one may solve for curvatures ϕ_z, ϕ_y the nonlinear system (18) and then the bending moment M_z can be simply evaluated using Eq. (19) and then $M_y = \tan(\alpha) M_z$. The moment-curvature diagram can be determined by continuously varying the strain in the reference point and solving iteratively the above problem for each reference strain $\varepsilon_c^{p,t}$:

$$\varepsilon_c^{p,t+1} = \varepsilon_c^{p,t} \pm \Delta\varepsilon_c; t = 1,2,3 \dots \qquad (22)$$

where $\Delta\varepsilon_c$ represents the incremental strain, usually assumed as $\Delta\varepsilon_c = 0.001$ in practical applications, $\varepsilon_c^{p,1}$ represents the initial value of the reference strain, and the sign $\pm$ in relation (22) denotes the sign assumed for compressive (-) and tensioned (+) fibre.

2.2.3 Moment curvature analysis: implementation details

Although the numerical procedure described above may be theoretically applied considering the origin of the reference axis in any position, for a specified bending moment ratio ($\tan(\alpha) = M_y/M_z$) and for high axial forces non-uniqueness or non-existence solutions may be exhibited when unsymmetrical (e.g. either geometrical or thermal) cross-section are analysed and the axial force falls outside the so-called iso-load contour (i.e. horizontal interaction diagram associated to ultimate strength capacity for a prescribed axial force) [11]. The reference strain and its initial value $\varepsilon_c^{p,1}$ may be selected as follows. First, a preliminary analysis is performed computing the axial strain (u) as the solution of the following nonlinear equation:

$$f(u) \equiv \int_{\boldsymbol{\Omega}} \sigma\left(\varepsilon_{mech}(u)\right) d\Omega + \Sigma_{b=1}^{N_b} \sigma\left(\varepsilon_{mech,b}(u)\right) A_{r,b} - N_0 = 0 \qquad (23)$$

where ε_{mech} is evaluated considering curvatures $\phi_z = 0, \phi_y = 0$, $\varepsilon_{tot}(u; T) = u = \varepsilon_{mech}(u) + \varepsilon_{th}(T)$ and represents the uniform strain field (i.e. at zero curvatures) that define an internal axial force in equilibrium with the prescribed axial force N_0. Next, when a given axial force N_0 is applied along with zero bending moments (M_{z0}=0 and M_{y0}=0) about the original centroid, the nonlinear system (12) is solved using the Newton iterative method, as outlined in [12], starting the iterative process with $u = u^*$ solution from the nonlinear equation (23), and setting $\phi_z = 0, \phi_y = 0$. The resulting curvatures serve as initial values for the curvatures associated with zero bending moments, ϕ_{z0}, ϕ_{y0} (see Eq. 13). These steps become unnecessary if the cross-section is symmetric or when considering a true plastic centroid as will be discussed later. To establish initial approximations for the curvatures (and implicitly for the reference fiber and reference strain $\varepsilon_c^{p,1}$), the nonlinear system (12) can be solved by considering small bending moments (i.e., λ=0.01 and M_y=tan$\alpha \cdot M_z$), with initial approximations for curvatures and axial strain taken as solutions from the preceding step when cross-section is referenced about original centroid and zero values may be assumed when cross-section is referenced about true plastic centroid. Once the initial reference strain and fiber are determined, the strain-driven procedure outlined earlier is applied successively until a limit value for the reference strain is reached. However, as already mentioned, when axial force falls outside the iso-load contour, the above technique is no longer applicable since no-solutions or multiple solutions may be exhibited. The following considerations attempt to illustrate the complexity of such situations. Having the axial strain (u^*), solution of the above nonlinear equation (23), and implicitly the strain field associated to the equilibrium, the resultant bending moment about original centroid may be simply evaluated by:

$$\overrightarrow{\mathbf{M}}_{int}^* = \int_\Omega \vec{\mathbf{r}} \times \vec{\sigma}(\vec{\mathbf{r}})d\Omega + \sum_{b=1}^{N_b} \vec{\mathbf{r}}_b \times \vec{\sigma}(\vec{\mathbf{r}}_b) = M_{z,int}^*\vec{\mathbf{i}} + M_{y,int}^*\vec{\mathbf{j}} \qquad (24)$$

with its components:

$$M_{z,int}^* = \int_\Omega \sigma\left(\varepsilon_{mech}(u^*)\right)yd\Omega + \sum_{b=1}^{N_b} \sigma\left(\varepsilon_{mech}(u^*)\right)y_b A_{r,b} \qquad (25)$$

$$M_{y,int}^* = -\int_\Omega \sigma\left(\varepsilon_{mech}(u^*)\right)zd\Omega - \sum_{b=1}^{N_b} \sigma\left(\varepsilon_{mech}(u^*)\right)z_b A_{r,b} \quad (26)$$

The new adaptive plastic centroid (APC) position ($\vec{\mathbf{e}} = e_z\vec{\mathbf{i}}+e_y\vec{\mathbf{j}}$) represents the location through which the axial force N_0 may be applied alone to produce pure axial stress with no bending [11]:

$$\overrightarrow{\mathbf{M}}_{APC} \equiv \overrightarrow{\mathbf{M}}_{int}^* - \vec{\mathbf{e}} \times \overrightarrow{\mathbf{N}}_0 = \vec{0} \qquad (27)$$

and may be evaluated by its eccentricities about the original centroid O as (Fig. 2a):

$$e_z = -\frac{M_{y,int}^*}{N_0} ; e_y = \frac{M_{z,int}^*}{N_0} \qquad (28)$$

The section response, reported at the original plastic centroid (O), subjected to axial force N_0 ($\overrightarrow{\mathbf{N}}_0 = N_0\vec{\mathbf{k}}$) and bi-axial bending moment with components (M_{zO}, M_{yO}), $\overrightarrow{\mathbf{M}}_O = M_{zO}\vec{\mathbf{i}} + M_{yO}\vec{\mathbf{j}}$ is equivalent with the section response reported at the new plastic centroid (APC) subjected to the same axial force and reduced bending moment $\overrightarrow{\mathbf{M}}_{APC} = M_{zAPC}\vec{\mathbf{i}} + M_{yAPC}\vec{\mathbf{j}}$: $\overrightarrow{\mathbf{M}}_{APC} = \overrightarrow{\mathbf{M}}_O - \vec{\mathbf{e}} \times \overrightarrow{\mathbf{N}}_0$ ($tan(\alpha_{APC}) = \frac{M_{yAPC}}{M_{zAPC}} \neq tan(\alpha) = \frac{M_{yO}}{M_{zO}}$) hence ($\overrightarrow{\mathbf{N}}_0, \overrightarrow{\mathbf{M}}_O$) and ($\overrightarrow{\mathbf{N}}_0, \overrightarrow{\mathbf{M}}_{APC}$) form an equivalent system of forces [11]. In other words, instead to solve the equilibrium about the original reference

9

centroid, the analysis can be conducted relative to the new plastic centroid. This approach facilitates selection of the initial approximations for curvatures as $\phi_z = 0, \phi_y = 0$ ensuring always numerically stable convergence since in this case axial force falls always within the load contour [11]. Furthermore, this representation can offer insights into situations of divergence encountered when seeking to maintain equilibrium around the original reference system (Fig. 2b): *divergent solutions arise when applied loads exceed the ultimate strength capacity of the cross-section, particularly when reduced loads are applied around the adaptive plastic centroid.*
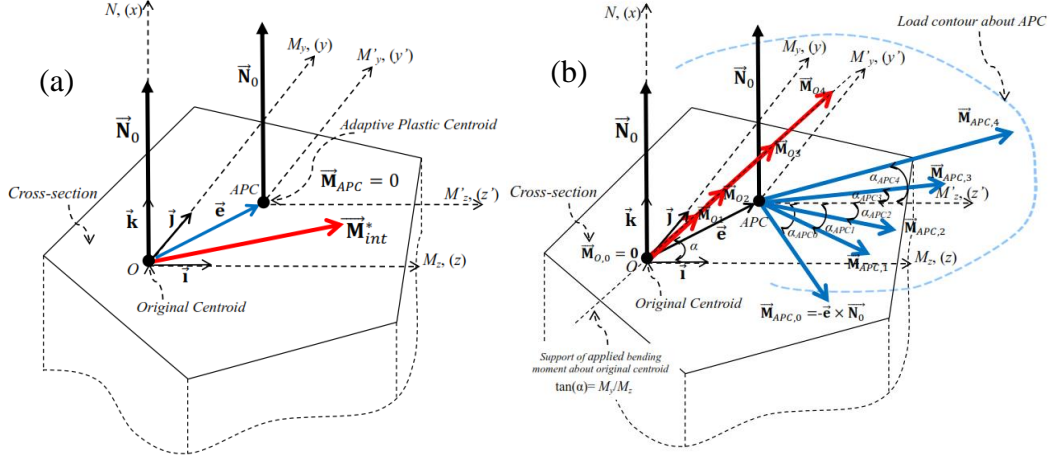
Figure 2: (a) Adaptive Plastic Centroid (APC); (b) Equivalent system of forces: original centroid vs. APC.

The present formulation is limited to scenarios where the axial force falls within the iso-load contour. Future advancements could explore extending this framework to encompass cases where the axial force deviates from this contour. Such enhancements would broaden the applicability of the model, enabling a more thorough examination of structural responses under diverse loading conditions.

3   Computational examples

For investigation of the computational efficiency, reliability and robustness of the proposed numerical methodology some computational and experimental examples are presented and discussed in the following.

3.1   Nonlinear Heat Transfer Analysis Verification

The first set of tests consists in comparisons of the predicted numerical results with a set of experimental results recorded in the tests carried out by Lie and Irwin [13] and those obtained by the numerical model developed in [4]. In the validation, the predictions of temperature-time given by the proposed model for several inner points of the concrete cross-section at different fire exposure times were compared with experimental values. Here, the concrete cross-section of 305x305 mm, exposed on four sides to a standard heating for 180 min has been considered. The cross-section has been subdivided into a 2033 three-nodded finite elements. For the main heat transfer parameters, the thermal values recommended in EN 1991-1-2 [1] are

used for siliceous concrete. The specific heat of concrete varies with temperature depending also on the moisture content. Specific heat at a moisture content of 4% as in [13] and both the lower and upper limit of thermal conductivity were used in the analysis. Although, the lower limit gives more realistic temperatures for normal strength concrete, the upper limit has been considered here for comparisons. Heat transfer from fire to element is assumed by convection and radiation on all sides with a convection factor of 25 W/m^{2}K and a resultant emissivity constant of 0.75. The predicted temperature-time curves at the location of the thermocouples placed at the cross-section are plotted against experimental points in Fig. 3. As it can be seen, the proposed model predicts well the evolution of the temperature along time when lower limit for concrete thermal conductivity is assumed. When upper limit is considered the predicted results slightly overestimate the temperature values.
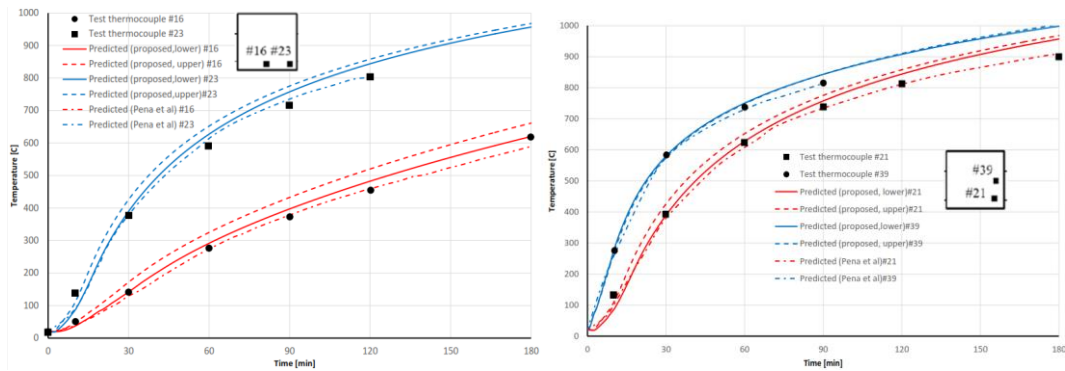
Figure 3: Temperature-time curves: predicted vs. experimental results.

3.2   Validation and Case Studies

Due to the lack of existence of explicit bi-axial moment curvatures diagrams, in the international literature, for cross-sections exposed to elevated temperatures the proposed method is indirectly validated by means of comparing the ultimate strength capacity diagrams retrieved from [9] with those generated with the proposed method adapted such that to provide the ultimate strength capacity. According with the proposed method, for a prescribed axial force and a given bending moment ratio the ultimate bending moments are obtained as a peak bending moments of the moment-curvature diagrams. The capacity diagrams are generated by successively applying moment curvature analysis for different values of α starting from 0° to 360° with an incremental angle of $\Delta\alpha=5^o$. The composite steel-concrete cross-section depicted in Fig. 4a [9, 11] consists of the concrete matrix, fifteen reinforcement bars of diameter 18 mm with 50 mm concrete cover, a structural steel element and a circular opening. The characteristic strengths, at ambient temperature, for concrete, structural steel and reinforcement bars are assumed as: f_c=17 MPa, f_{ys}=323MPa, f_{yr}=400MPa, respectively and the Young modulus for all steel sections was 200 GPa. The entire external section surface is subjected to the ISO 8364 standard fire, whereas the internal surface associated to the void was assumed to be adiabatic. A convection factor of 25W/(m^{2}K) and a resultant emissivity of 0.7 have been used. The cross-section has been subdivided into a 2018 total number of three-nodded finite elements (Fig. 4b), and the mechanical and thermal properties for concrete are taken

11

from Eurocode 2 for siliceous aggregates with 0% moisture and lower limit of thermal conductivity.
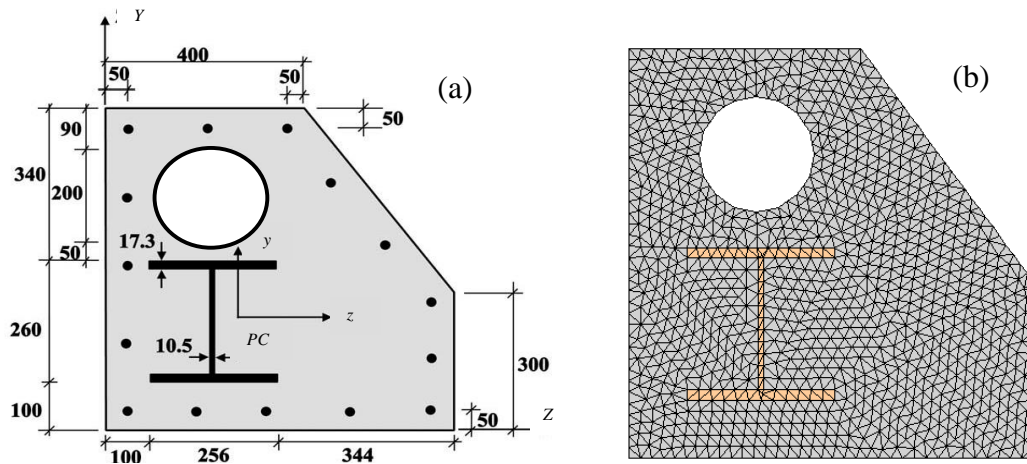
Figure 4: (a) Composite steel-concrete cross-section; (b) Finite element mesh.

A linear descending branch for concrete in compression has been assumed in all computational examples. In the analysis conducted in [9] the heat transfer analysis did not account for the steel section. To ensure consistency and relevance in our analyses and comparisons of the results, it was incorporated this modelling detail, in the heat transfer analysis. The temperature field for 300 minutes of fire exposure is depicted in Fig. 5a. The comparative moment capacity diagrams (load contour determined about plastic centroid at ambient temperature), for a compressive value of axial force equal with 4120 kN, for several exposure times (30, 90, 180 and 300 min) are depicted in Fig. 5b. As it can be seen a very close agreement between this study results and those given in [9] may be noted.
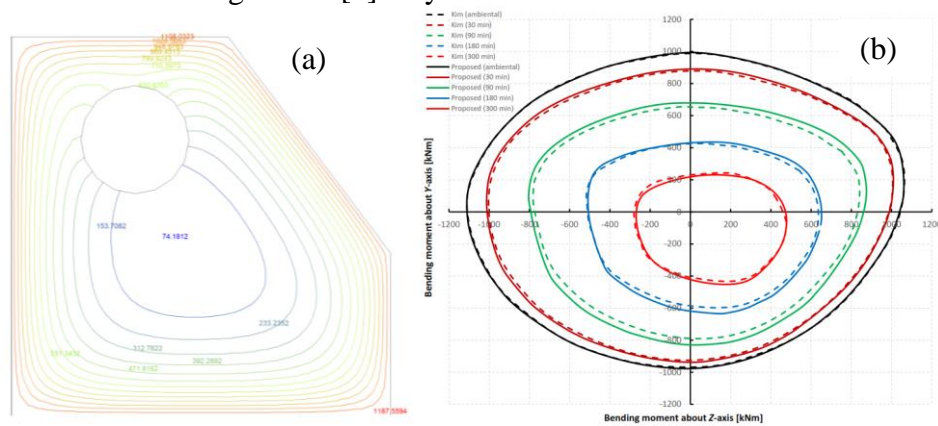
Figure 5: (a) Temperature field distribution at 300 minutes of fire exposure;
(b) Moment capacity diagrams for a compressive axial force N=-4120 kN.

This comparison proves the accuracy of the proposed numerical methodology in assessment of the ultimate strength capacity of composite cross-sections subjected to bi-axial bending moment and compressive axial force. Figure 6a depicts the moment-curvature diagrams generated based on the implemented method

12

considering biaxial bending (α=30º) and different exposure times and for a prescribed axial force (*N*=-4120 kN).
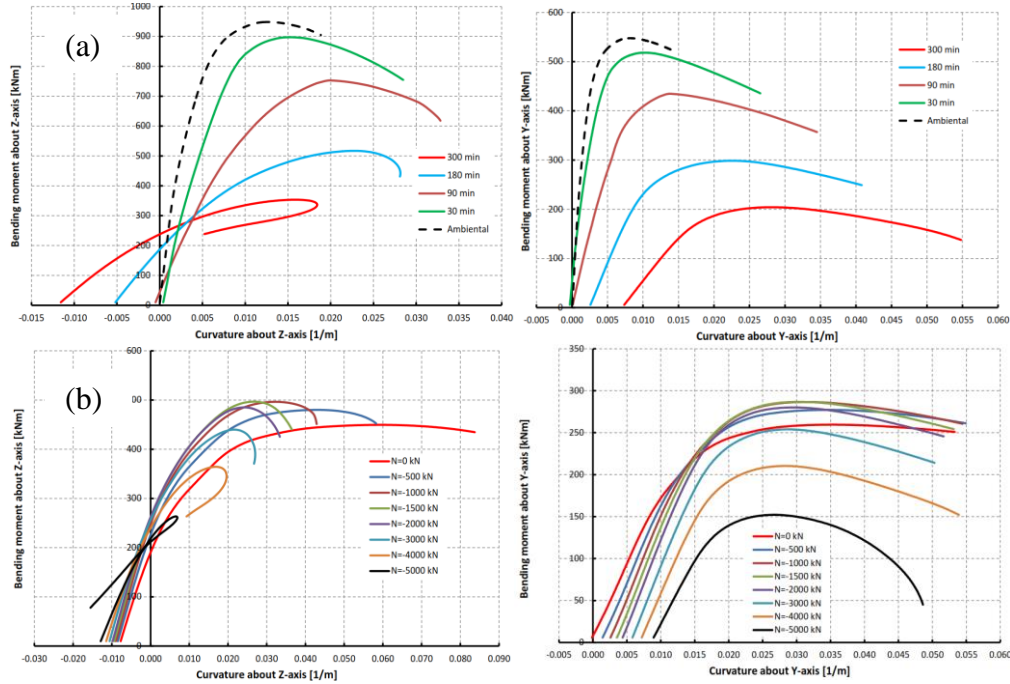
Figure 6: Moment-curvature diagrams of composite cross-section.

As it can be seen significant reduction in both strength and stiffness of cross-section is revealed as time of exposure increase. The influence of the axial force level (compression) over inelastic response of cross-section is presented in Fig. 6b where for the same time of fire exposure (300 minutes) different levels of compressed axial force are considered while keeping constant bending moment ratio (α=30º). Furthermore, this study demonstrates the capability of the proposed numerical approach to assess the complete inelastic behaviour of the cross-section, including advanced post-critical domain phenomena such as softening and the snap-back effect.

4   Conclusions and Contributions

This paper has presented a new computational method for evaluating the complete moment-curvature response of composite steel-concrete cross-sections with arbitrary shapes exposed to elevated temperatures. The diagrams are determined such that axial force and bending moment ratio are kept constant($M_\alpha - N - \phi$). The proposed approach introduces a "fail-safe" methodology by integrating the strain-driven control and damped iterative Newton approach to enhance global convergence properties. A sequentially coupled thermal-stress analysis was implemented: first, a thermal-sectional analysis (i.e. a nonlinear transient heat transfer finite element analysis) is carried out and then the moment-curvature analysis is solved. Both thermal and mechanical analyses are implemented within the same software environment (.NET) with full graphical interface. Addressing crucial computational

13

challenges, the study explores various aspects, including the occurrence of non-uniqueness or non-existence of solutions observed when analysing unsymmetrical composite cross-sections and when the axial force falls outside the so-called iso-load contour. It correlates these pathological behaviours with divergent solutions due to the surpassing of resistance capacity in relation to the adaptive plastic centroid. The validation process has involved comparisons with other numerical and experimental results from international literature, extending also the benchmark results used for assessing the strength capacity and complete moment-curvature diagrams of composite cross-sections under high temperature conditions.

References

[1] EN 1992-1-2, „Eurocode 2: Design of concrete structures, part 1.2: General rules, Structural Fire Design. BS", 2004.

[2] EN 1993-1-2, „Eurocode 3: Design of steel structures-Part 1-2: General rules-Structural fire design", CEN; 2005.

[3] EN 1994-1-2, "Eurocode 4: Design of composite steel and concrete structures-Part 1-2: General rules-Structural fire design" CEN, 2005.

[4] D.L. Pena, V. Albero, C. Ibanez, A. Hospitaler, „Sectional model for the fire evaluation of reinfirced concrete columns subjected to biaxial bending", Engineering Structures, 247, 2021.

[5] C. Yu, Z. Huang, I.W. Burgess, R.J. Plank, „Development and validation of 3D composite structural elements at elevated temperatures", Journal of Structural Engineering, 136 (3): 275-284, 2010

[6] V.K. Papnikolau, „Analysis of arbitrary composite sections in biaxial bending and axial load", Computers and Structures, (98-99): 33-54, 2012

[7] C.G. Chiorean, „A computer method for moment-curvature analysis of composite steel-concrete cross-sections of arbitrary shape", Engineering Structures and Technologies, 9(1): 25-40, 2017.

[8] I.J.M Lemes, P.H.A. Lima, R.C. Barros, R.A.M. Silveira, C.G. Chiorean, „A complete assessment of the moment-curvature relationship of compressed steel-concrete composite cross-sections", ce/papers, 5(4): 819-827, 2022.

[9] H.S. Kim, „Obtaining interaction diagram of concrete section exposed to fire by mathematical optimization", Journal of Building Engineering, 44, 2021.

[10] D. Medall, A. Espinos, V. Alberto, M.L. Romero, "Simplified proposal for the temperature field of steel-reinforced CFST columns exposed to fire", Engineering Structures, 273 (115083), 2022.

[11] C.G. Chiorean, "Computational issues in biaxial bending capacity assessment of RC and composite cross-sections exposed to fire", Computers & Structures, 2024 (revision submitted).

[12] C.G. Chiorean, „A Computer Method for Nonlinear Inelastic Analysis of 3D Composite Steel-Concrete Frame Structures", Engineering Structures, 57: 125-152, 2013.

[13] T. Lie, R. Irwin, „Evaluation of the fire resistance of reinforced concrete columns with rectangular cross- sections". Internal Report 601, Institute for Research in Construction, NRC Canada, 1990, Ottawa, Canada.